Available online at www.sciencedirect.com
ScienceDirect
Ceramics International 38 (2012) 177–188
CERAMICS INTERNATIONAL
www.elsevier.com/locate/ceramint

Synthesis, characterization and microbiological response of silver doped bioactive glass nanoparticles

Abeer M. El-Kady [a,c,*], Ashraf F. Ali [b,c], Rizk A. Rizk [d], Manar M. Ahmed [a]

[a] Biomaterials Department, National Research Center, 33 El-Bohooth St., Dokki 12622, Cairo, Egypt
[b] Inorganic Chemistry Department, National Research Center, 33 El-Bohooth St., Dokki 12622, Cairo, Egypt
[c] Advanced Materials and Nanotechnology Lab., Center of Excellence, National Research Center, Dokki 12622, Cairo, Egypt
[d] Physics Department, Faculty of Science, Helwan University, Cairo, Egypt

Received 20 August 2010; received in revised form 15 March 2011; accepted 28 May 2011
Available online 1st July 2011

Abstract

Glass nanoparticles containing 1, 3, 5, and 10 wt% of Ag_2O (coded; GAg1%, GAg3%, GAg5%, and GAg10%, respectively) were synthesized through a quick alkali mediated sol–gel method and were characterized by TEM, XRF, FT-IR, XRD, TGA, and DSC. Thermal analysis showed that all organic and inorganic by-products were completely decomposed before 700 °C and, hence, all glass samples were stabilized at this temperature. XRD confirmed the amorphous nature of all glasses after stabilization. TEM micrographs showed that the average particle sizes of all samples were less than 100 nm in diameter and the XRF showed that the compositions of the obtained glasses were almost consistent with the designed ones. The samples GAg1%, GAg3%, GAg5%, and GAg10%, showed average pore diameters of 19.85, 18.22, 13.32, and 19.62 nm and specific surface areas of 73.18, 100.38, 192.6, and 55.7 m^2/g, respectively. In addition, their porosity% was 76.53, 83.20, 77.97, and 79.61%, respectively. The FT-IR spectra of all glasses showed bands located in the range of 1000–1200, 725–800, and 450–480 cm^{-1} that correspond to the Si–O–Si asymmetric stretching vibration, the Si–O–Si symmetric stretching vibration, and the Si–O–Si bending mode, respectively. Finally, all samples had an anti-bacterial effect against different types of bacteria and the extraction of silver ions from them followed a diffusion-controlled mechanism, which could demonstrate their ability to treat bone infection.

Keywords: Bioactive glass nanoparticles; Silver; Sol–gel processes; Bone treatment; Antibacterial

1. Introduction

Bioactive glasses were used extensively as an orthopedic and dental grafting materials, and as a tissue engineering scaffolds [1–4]. The original bioactive glasses were prepared through melting mixture of the related oxide precursors at relatively high temperatures [5]. However, advances in sol–gel processing technology have allowed the manufacture of a new generation of bioactive glasses at lower temperatures [6–9]. Results from both *in vitro* studies in simulated body fluid [10–12] and *in vivo* tests in animals showed that the sol–gel derived bioactive glasses were more bioactive and degradable than melt-derived ones [13].

One major complication for bone reconstruction is the development of bacterial infection. Removal of the infected bone tissues leaves behind large bone defects which need an orthopedic implant to heal. Ideally, the implant should have the ability to regenerate bone tissue and to treat the infection by delivering an antibacterial agent in a controlled and continuous manner. The localized release of an anti-bacterial agent at the surgical site could provide a targeted treatment for the infection. The anti-bacterial effect of silver ion was well documented [14–16]. It was found to be highly toxic to microorganisms, and showed a strong biocidal effects on 12 species of bacteria including *E. coli* [17,18]. Bioactive glasses containing silver as an antibacterial agent have attracted a significant attention in recent years [19–21]. The incorporating of silver ions into the glass matrix allowed the controlled delivery of this anti-bacterial agent at the site of the bone infection.

Reducing the particle size of materials to nano-size has showed to improve their biological properties and their grain

* Corresponding author at: Biomaterials Department, National Research Center, 33 El-Bohooth St., Dokki 12622, Cairo, Egypt.
Tel.: +20 2 333 70933; fax: +20 2 333 70931.
E-mail address: abeerelkady_2000@yahoo.co.uk (A.M. El-Kady).

0272-8842/$36.00
doi:10.1016/j.ceramint.2011.05.158

size was found to influence their ability to promote bone growth [22–24]. Several studies have provided significant evidences that ceramics, metals, polymers, and composites with nanometer grain sizes selectively enhanced osteoblast function, and hence, lead to more bone growth than materials with micrometer grain size [25–28]. Therefore, the main objective of the present study was to engineer silver-releasing bioactive glass nanoparticles with a predicted, as well as a controlled, silver releasing rate to suit different medical cases facing the surgeon. Different concentrations of silver oxide were incorporated in the structure of glass nanoparticles in order to promote an antibacterial effect of the materials to treat bone infection. In addition, silver ion releasing profile and its inhibitory effect on different types of bacteria were evaluated.

2. Materials and methods

2.1. Materials

Tetraethyl orthosilicate (TEOS), calcium nitrate tetrahydrate $Ca(NO)_3{\cdot}4H_2O$, silver nitrate $AgNO_3$, and triethyl phosphate (TEP) were all ≥98% and were purchased from Fluka (Buchs, Switzerland). Ammonia solution, 33%, and nitric acid, 68%, were purchased from Merck, USA. Both nitric acid and ammonia solutions were diluted to 2 M using distilled water.

2.2. Sol–gel synthesis of silver-doped bioactive glass nanoparticles

Bioactive glass nanoparticles containing 1, 3, 5 and 10 wt% of Ag_2O were synthesized through a quick alkali-mediated sol–gel technique [29,30]. Ag_2O was added to the glass compositions at the expense of CaO. Table 1 lists the nominal compositions and codes of the prepared glasses. Initially, tetraethyl orthosilicate, distilled water, 2 M nitric acid (as a hydrolysis catalyst), were successively mixed in ethanol and the mixture was allowed to react for 60 min under continuous magnetic stirring for the acid hydrolysis of TEOS. Then appropriate amounts of series of reagents were added in the following sequence: (TEP), $Ca(NO_3)_2{\cdot}4H_2O$, $AgNO_3$, allowing 30 min for each reagent to react completely. After the final addition, mixing was continued for 60 min to allow for the completion of hydrolysis. The mixture was then moved into a conventional ultrasonic bath (working at a frequency of 50–60 kHz, 100/200 W), and 2 M ammonia solution (a gelation catalyst) was dropped into the mixture while vigorously agitated with a mechanical stirrer. Gelation of the mixture took place in a few minutes. The combination of an ultrasonic vibration and a mechanical agitation of the mixture during gelation were conducted to prevent the formation of a bulk gel. Finally, each prepared gel was dried at 75 °C for 2 days in a drying oven. According to the results of the thermal analysis of the dry gels, which showed that there was no further weight loss above 700 °C, the gels were stabilized by heat treatment, at a constant heating rate of 3 °C min^{-1} up to 700 °C.

Table 1
The nominal compositions and codes of the prepared silver doped sol–gel bioactive glasses nanoparticles.

Sample code	Composition (wt%)			
	SiO_2	CaO	P_2O_5	Ag_2O
GAg1%	58	32	9	1
GAg3%	58	30	9	3
GAg5%	58	28	9	5
GAg10%	58	23	9	10

2.3. Characterization

Thermogravimetric analyses (TGA), and differential calorimetric analyses (DSC) were performed for the dried gels using a computerized 7 series USA PerkinElmer thermal analysis system. Scans were performed in the air atmosphere, and in a temperature range of 50–1000 °C, at a rate of 10 °C min^{-1}. The materials were analyzed using aluminum oxide powder as a reference. The phase analysis of the samples was examined by X-ray diffractometer, model BRUKER axs, D8ADVANCE, and employing a Ni-filtered Cu Kα irradiation at 40 kV and 25 mA. The morphology and particle size of the glass powders were analyzed using TEM (JEM2010, Japan) working at 200 kV. The elemental composition of the glass powders was determined by energy dispersive X-ray analysis (JEOL JXA-840A, Electron probe micro-analyzer). The infrared spectra of the prepared glasses were obtained using a Fourier transformer infrared spectrophotometer (FT-IR) (model FT/IR-6100 type A). The spectra were recorded in a wave number range of 400–4000 cm^{-1}. Nitrogen adsorption–desorption isotherms were measured with a high-speed gas sorption analyzer (NOVA 2000 series, Chromatic, UK) at 77 K. The Barrett–Emmett–Teller (BET) method was utilized to calculate the specific surface areas. The pore volumes, average pore diameters and pore-size distributions were derived from the adsorption branches of the isotherms using the Barrett–Joyner–Halanda (BJH) method. The total pore volumes were estimated from the amount adsorbed at a maximum relative pressure. The porosity percent and bulk densities were determined using the mercury intrusion porosimetry technique (19321, Micrometric, USA).

2.4. Degradation study

2.4.1. Weight loss

Silver-doped sol–gel bioactive glass disks (5 mm diameter and 2 mm thickness) with different silver contents (1, 3, 5, and 10 wt%) were prepared and placed in plastic container which was filled with 30 ml of simulated body fluid (SBF) and placed in an incubator at 37 °C for different time periods (24, 72, 168 and 336 h). The SBF had a composition and an ionic concentration almost equal to human plasma. The inorganic ion concentrations in SBF were: Na^+ 142.0 mM, K^+ 5.0 mM, Ca^{2+} 2.5 mM, Mg^{2+} 1.5 mM, Cl^- 148.0 mM, HCO_3^- 4.2 mM, HPO_4^{2-} 1.0 mM, SO_4^{2-} 0.5 mM. The solution was buffered at pH 7.4 with tris(hydroxymethyl) aminomethane and 1 M HCl at 37 °C [31]. The disks were removed from SBF and left to dry at 100 °C for 6 h, and then left to cool down to room temperature before they

were weighted. Weight loss% (WL) of each sample was calculated according to the following equation (1):

$$\mathrm{WL} = \left[\frac{M_0 - M_t}{M_0}\right] \times 100 \quad (1)$$

where M_0 was the initial weight of each sample and M_t was the weight of the same sample measured at time t after being dried. Moreover, at selected intervals, the concentrations of silver and silica ions in the SBF were measured using an inductively coupled plasma atomic emission spectrometer (SPS-1500 VR, Seiko Instruments Inc., Tokyo, Japan).

2.4.2. Modeling of glasses dissolution and silver release kinetics

In order to predict the release rate of silver from the glasses surface, it was necessary to fit the dissolution data to a suitable model. Many mathematical models were proposed to describe the corrosion of alkali-silicate glasses in aqueous solutions. The more commonly used one was the heterogeneous model [32]. In that model, the corrosion of the glass in aqueous solution is governed by two stages; namely, the diffusion-controlled ion exchange and the dissolution of the glass network. In the first stage, ion exchange involves the replacement of alkali ions in the glass by hydronium ions (H_3O^+) from the solution and the extraction of ions varied with the square root of time. On the other hand, the corrosion process in the second stage was controlled mainly by the glass dissolution and the extraction of ions was linear with time. The extraction of ions during the first stage of heterogeneous model could be expressed by the following equation (2):

$$Q = kt^{1/2} \quad (2)$$

where Q is the cumulative ion concentration released in aqueous solution, t is the leaching time in hour, and k is the dissolution rate constant. To determine the dissolution rate of silver and silica, and to see if their profiles of dissolution has fitted the heterogeneous model, Q was plotted against $t^{1/2}$ and a linear regression analysis of the dissolution data was carried out, and a straight line was fitted through the data where the slope of that line gives the rate of ion dissolution. In addition, the correlation coefficient (R^2) of the cumulative ion concentration released versus the square root of time was determined. R^2 is a statistical measure of how well the regression line approximates the real dissolution data. The glass dissolution was considered to follow the heterogeneous model if R^2 was higher than 0.95.

2.5. Microbiological analysis

Inhibition of bacterial growth by the silver-doped bioactive glasses was investigated using a disk diffusion methodology (BSAC Disk Diffusion Method for Antimicrobial Susceptibility Testing, Version 4, 2005). Isosensitest agar (Oxoid, Basingstoke, UK) plates were inoculated with a standardized culture of *Staphylococcus aureus* (ATCC 25923) or *E. coli* (NCTC 10418). Glasses disks of 5 mm diameter and 2 mm thickness were then placed onto the inoculated plates. Those plates were incubated overnight in air at 37 °C. The diameters of any inhibition zones formed around the disks were measured.

2.6. Statistical analysis

All data were expressed as the means ± standard deviation (SD) for $n = 6$ and were analyzed using standard analysis of student's t-test. The level of significance was set at $p < 0.05$.

3. Results

3.1. Characterization

3.1.1. TEM

Fig. 1 shows the TEM photos of the samples GAg1%, GAg3%, GAg5%, and GAg10% (photos a, b, c, and d, respectively). As could be seen from the figure the grain size of all glass samples was less than 100 nm.

3.1.2. Energy-dispersive X-ray (EDX) analysis

The EDX analysis was carried out for the silver doped bioactive glass nanoparticles to verify that they contained silver. The EDX analysis of samples GAg1%, GAg3%, GAg5%, and GAg10% are shown in Fig. 1 (e, f, g and h, respectively). All samples showed silica, calcium, and phosphorous peaks which was typical for any silicate bioactive glasses. The EDX analysis showed that a silver peak was present in all the glass samples. Moreover, the analysis showed that its intensity was increased, while that of calcium decreased as the silver content was increased in the glasses. This is because CaO was substituted by Ag_2O (on wt% bases) in the glass compositions.

3.1.3. Thermal analysis

Thermogravimetric analysis (TGA), and differential scanning calorimetric analysis (DSC), curves for samples GAg1%, GAg3%, GAg5%, and GAg10% are shown in Fig. 2. For the first three samples, the TGA curves showed three mass losses after heating from room temperature to 1000 °C. Those weight losses appeared at the temperature intervals of 30–175, 175–320, and 320–600 °C. The first weight loss was attributed to the elimination of residual alcohol and physically adsorbed humidity water from the pores of the gel. This was reflected in the DSC curves of samples GAg1%, GAg3%, and GAg5% as the first large endothermic peak centered around 119, 105 and 111 °C, respectively [30,33]. The second weight loss was reflected in the exothermic peaks in the DSC curves of all of the three samples and centered at 272, 253, and 237 °C for samples GAg1%, GAg3%, and GAg5%, respectively, which was most likely due to desorption of chemically adsorbed water [34]. The third weight loss that was shown by their TGA curves was due to the decomposition of nitrates NO_3^- [11]. The endothermic peaks centered around 533, 535, and 528 °C on the DSC curves of samples GAg1%, GAg3%, and GAg5%, respectively, was due to that decomposition. On the other hand the TGA curve for sample GAg10% showed four weight losses

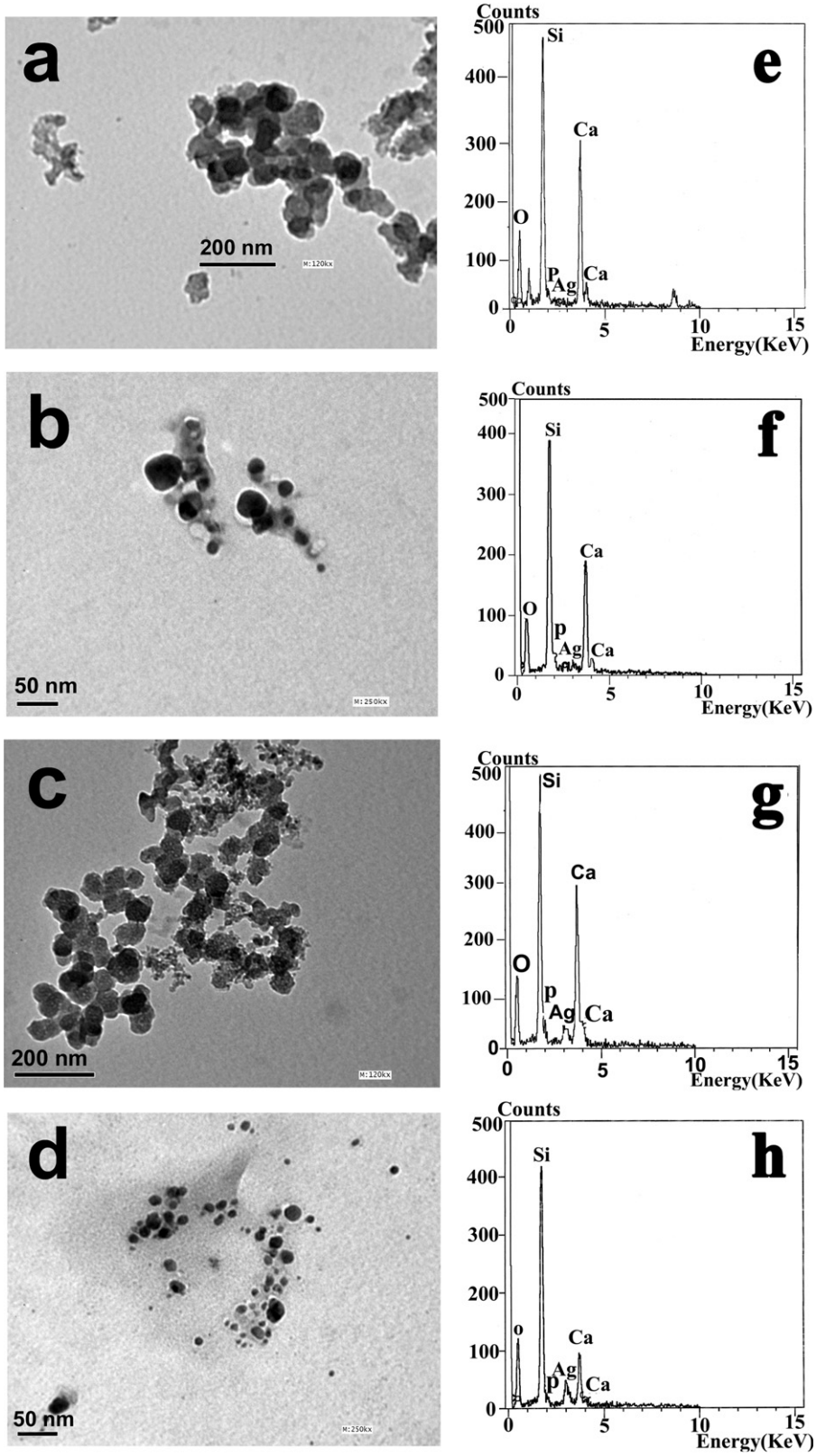

Fig. 1. TEM photos of the Ag-doped bioactive glass nanoparticles containing 1, 3, 5, and 10 wt% of silver oxide (photos a, b, c, and d, respectively) and their corresponding EDX analysis (photos e, f, g and h, respectively).

as the heating process proceeded from room temperature to 1000 °C. Those weight losses appeared at the temperature intervals of 30–160, 160–255, 255–415, and 415–600 °C. The first weight loss was attributed to the elimination of residual alcohol and physically adsorbed humidity water. The second and third weight losses were reflected in the exothermic peaks that appeared in the DSC curve of sample GAg10% and were centered at 233 and 324 °C, respectively, which were probably

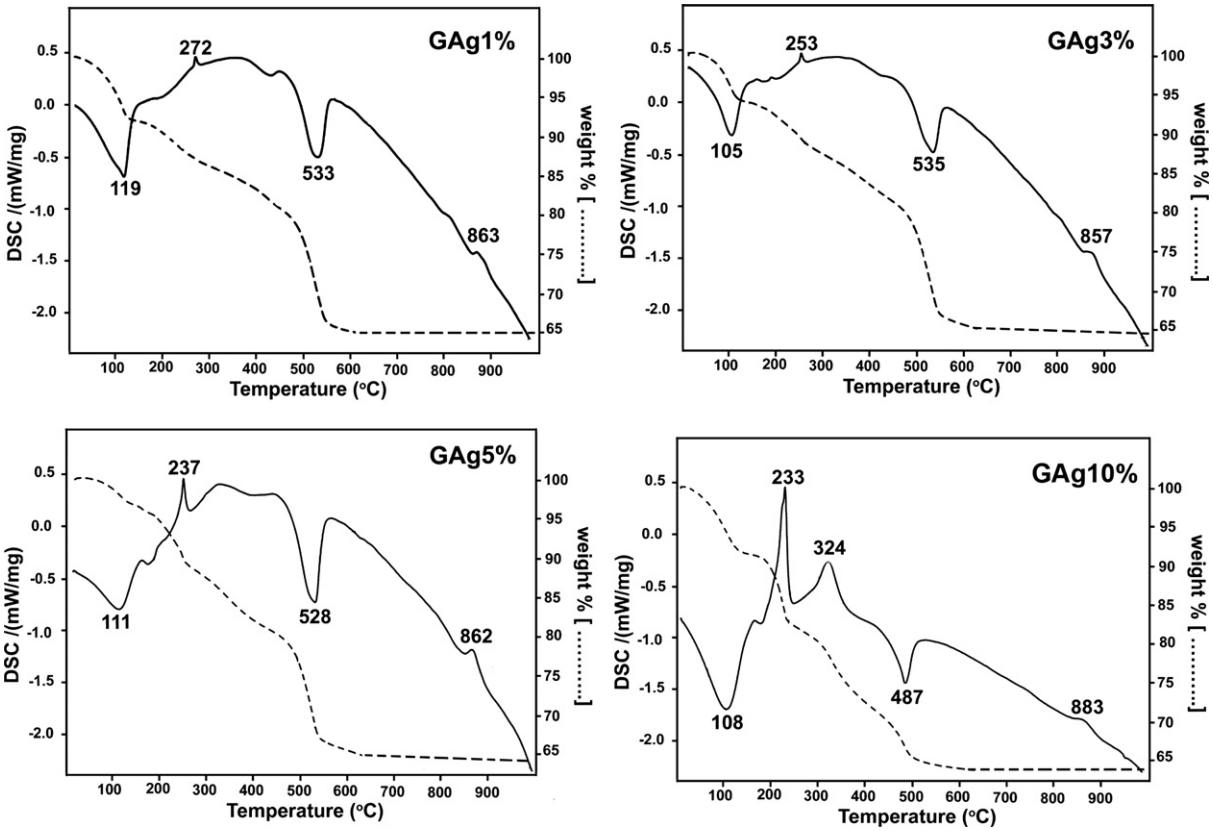

Fig. 2. TGA and DSC curves for the samples GAg1%, GAg3%, GAg5% and GAg10%.

due to the desorption of chemically adsorbed water and/or to the loss of organics (i.e. alkoxy groups) [11]. The fourth weight was due to the decomposition of nitrates NO_3^- [34]. This was reflected in the DSC curve of sample GAg10%, as an endothermic peak centered at 487 °C. The above results confirmed that all residuals could be removed before 700 °C. Therefore, the temperature of 700 °C was chosen for the stabilization of all the glass powders. The final exothermic peak, located on the DSC curves for samples GAg1%, GAg3%, GAg5%, and GAg10% at 863, 857, 862, and 883 °C, respectively was due to the glass crystallization into glass-ceramic [35].

3.1.4. XRF

The quantitative analysis (wt%) of the silver doped bioactive glass powders, was measured by XRF and was compared to that of the designed compositions (see Table 2). The results showed that the compositions of the obtained glasses were almost consistent with the designed ones, which indicated that the glass compositions were not affected by the rapid gelation during synthesis.

3.1.5. FT-IR

FT-IR spectra of silver doped glass samples are shown in Fig. 3. For all glass powders, the band located in the range of 1000–1200 cm^{-1} correspond to Si–O–Si asymmetric stretching vibration, whereas the band observed in the range of 725–800 cm^{-1} was attributed to the Si–O–S symmetric stretching vibration. In addition, band located in the range of 450–480 cm^{-1} was ascribed to the [Si–O–Si] bending mode [30,36].

3.1.6. Textural analysis

The N_2 adsorption isotherms of samples GAg1%, GAg3%, GAg5% and GAg10% are plotted in Fig. 4 (a, b, c, and d,

Table 2
The quantitative analysis of the composition (wt%) of the silver doped bioactive glass nanoparticles, measured by XRF, as compared to that of the designed compositions.

Constituents	GAg1% (wt%)		Gag3% (wt%)		GAg5% (wt%)		GAg10% (wt%)	
	Design	Experiment	Design	Experiment	Design	Experiment	Design	Experiment
SiO_2	58	57.6	58	57.2	58	57.3	58	58.7
CaO	32	31.4	30	30.6	28	29.1	23	22.7
P_2O_5	9	9.66	9	8.7	9	8.4	9	8.8
Ag_2O	1	1.1	3	3.3	5	4.6	10	9.7
Impurity	–	0.2	–	0.2	–	0.5	–	0.2

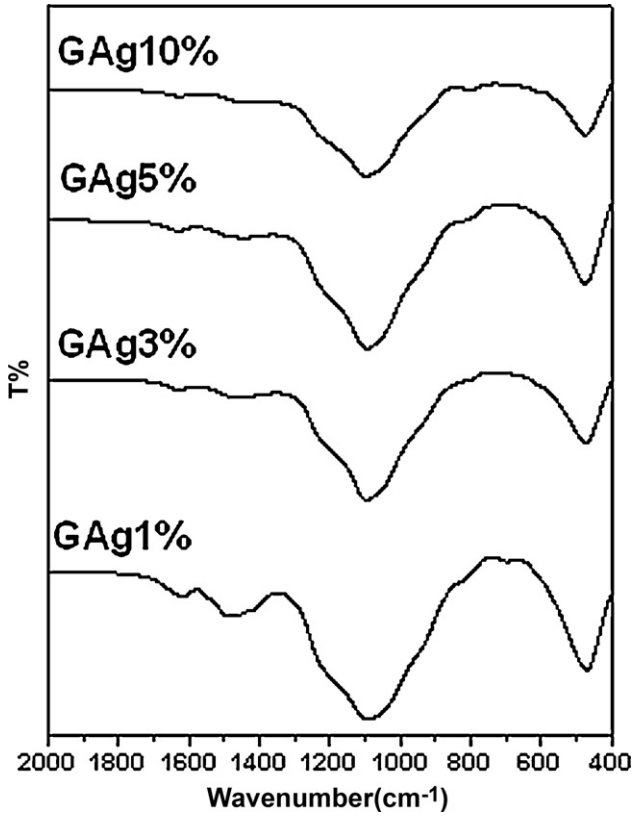

Fig. 3. FTIR spectra of samples GAg1%, GAg3%, GAg5% and GAg10%.

respectively). They correspond to the type IV isotherm according to the IUPAC classification [37]. The characteristic hysteresis loop of that isotherm could be observed in all samples, where the desorption branch did not follow the same path as that of the adsorption branch at relatively high P/P_0 values. This behavior clearly indicates the presence of mesopores in all samples. The isotherms had a type H3 hysteresis loops that was associated with slit-shape mesopores according to the IUPAC classification [37]. The pore size distributions were obtained from the desorption branch of the isotherm for samples GAg1%, GAg3%, GAg5% and GAg10% and are shown in Fig. 4 as e, f, g and h, respectively. All the samples showed a broad pore size distribution in the mesopore range ($2 <$ pore diameter < 50 nm). The average pore diameters in the mesopore range for samples GAg1%, GAg3%, GAg5% and GAg10% were 19.85, 18.22, 13.32, and 19.62 nm, respectively. Samples GAg1% and GAg10% showed a biomodal pore size distribution while samples GAg3% and GAg5% showed a monomodal distribution. The bimodal distribution could infer the presence of pores with two different sizes or narrowing into the pores [36]. The specific surface areas of the glasses were 73.18, 100.38, 192.6, and 55.7 m^2/g for samples GAg1%, GAg3% GAg5%, and GAg10%, respectively. All glasses powders had relatively high surface area and porosity%. The porosity% was 76.53, 83.20, 77.97, and 79.61% for samples GAg1%, GAg3%, GAg5%, and GAg10%, respectively. Table 3 summarizes all the data of their textural analysis.

3.1.7. XRD

The X-ray diffraction patterns of the as prepared dry gels and after being calcined at 700 °C for 3 h are shown in Fig. 5(a) and (b), respectively. The XRD patterns confirmed the amorphous nature of all glasses after stabilization.

3.2. Degradation study

3.2.1. Weight loss

The change of weight losses% of GAg1%, GAg3%, GAg5%, and GAg10% with time of immersion is shown in Fig. 6. After 24 h of immersion, the difference in weight loss between all samples was not significant ($p > 0.05$). However, samples GAg1% and GAg3% had significantly greater weight losses ($p < 0.05$), than samples GAg5% and GAg10% at 72, 168 and 336 h. The final weight losses were 17.12, 16.18, 13.71, and 8.99% for samples GAg1%, GAg3% GAg5%, and GAg10%, respectively.

3.2.2. Modeling of glasses dissolution and silver release kinetics

The change of the cumulative concentration of silver ion, released from all glass samples into the SBF, with time and with the square root of time are shown in Fig. 7(a) and (b), respectively. Those data showed that the difference in concentration of silver ions released from all samples was not significant ($p > 0.05$), at 24 and 72 h. However, samples GAg1% and GAg3% significantly ($p < 0.05$), released more silver ions than samples GAg5% and GAg10% at 168 and 336 h. In addition, sample GAg5% significantly ($p < 0.05$), released more silver ions than sample GAg10% at 168 and 336 h. The rate of silver release versus silver content in the glasses is shown in Fig. 8. The results showed that the rate of silver ions release was correlated to the silver content. For the sample GAg10%, the rate of silver ions release was significantly ($p < 0.05$), decreased as compared to that of glasses of less silver contents. The silver ions release rates for samples GAg1%, GAg3%, GAg5%, and GAg10% were 0.49,

Table 3
The data of the textural analysis carried out for GAg1%, GAg3%, GAg5%, and GAg10%.

Sample code	Average. pore diameter (nm)	Total pore volume (cm^3/g)	Bulk density (g/ml)	Total porosity (%)	Surface area (m^2/g)
GAg1%	19.9	0.04	0.67	76	73
GAg3%	18.2	0.05	0.61	83	100
GAg5%	13.3	0.06	0.60	77	192
GAg10%	19.6	0.03	0.63	79	55

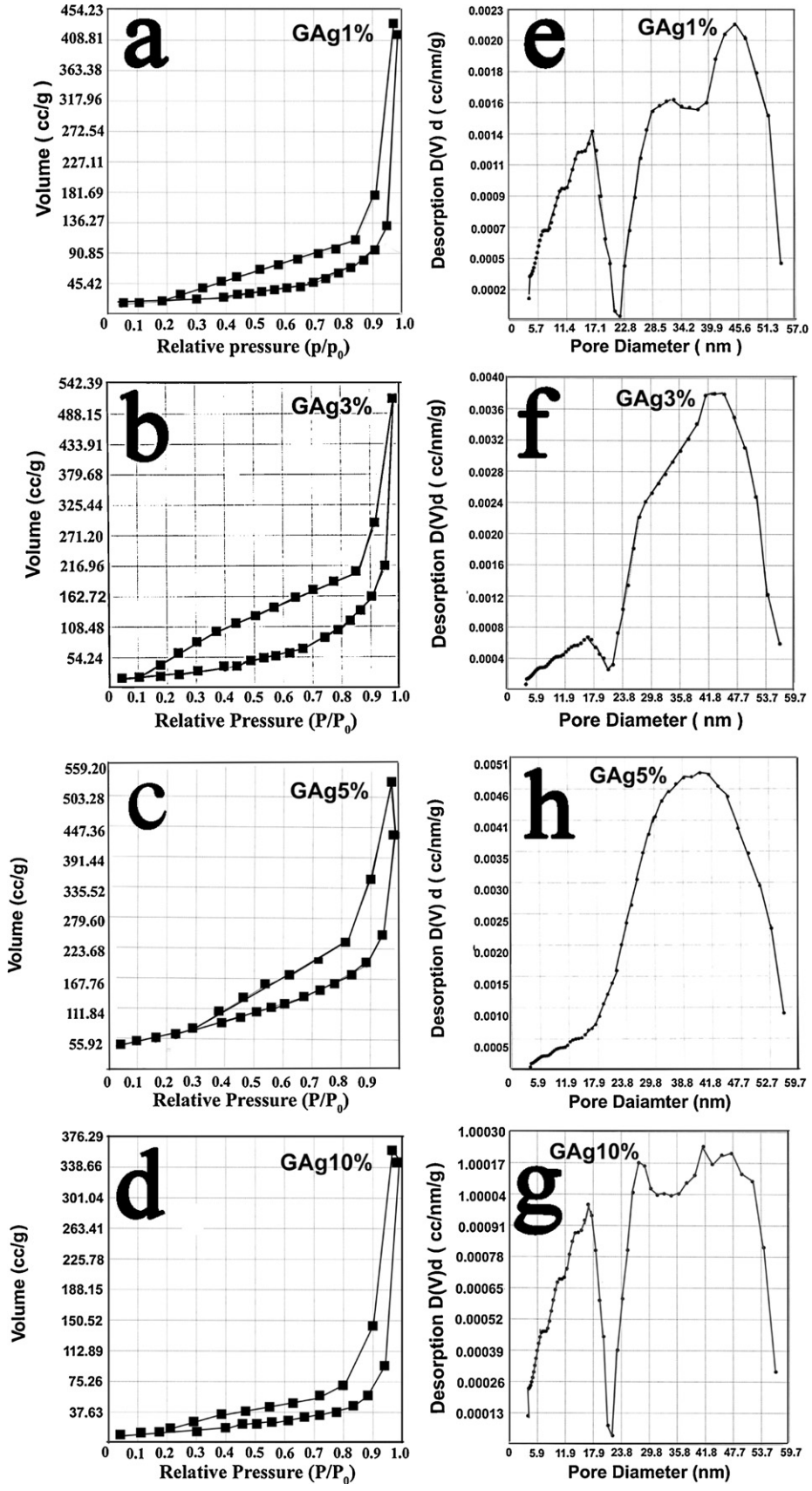

Fig. 4. The nitrogen adsorption–desorption isotherms of samples GAg1%, GAg3%, GAg5% and GAg10% (a, b, c and d, respectively), they were characterized by type IV isotherm according to the IUPAC classification. The corresponding pore size distributions are shown as plots e, f, g, and h, respectively.

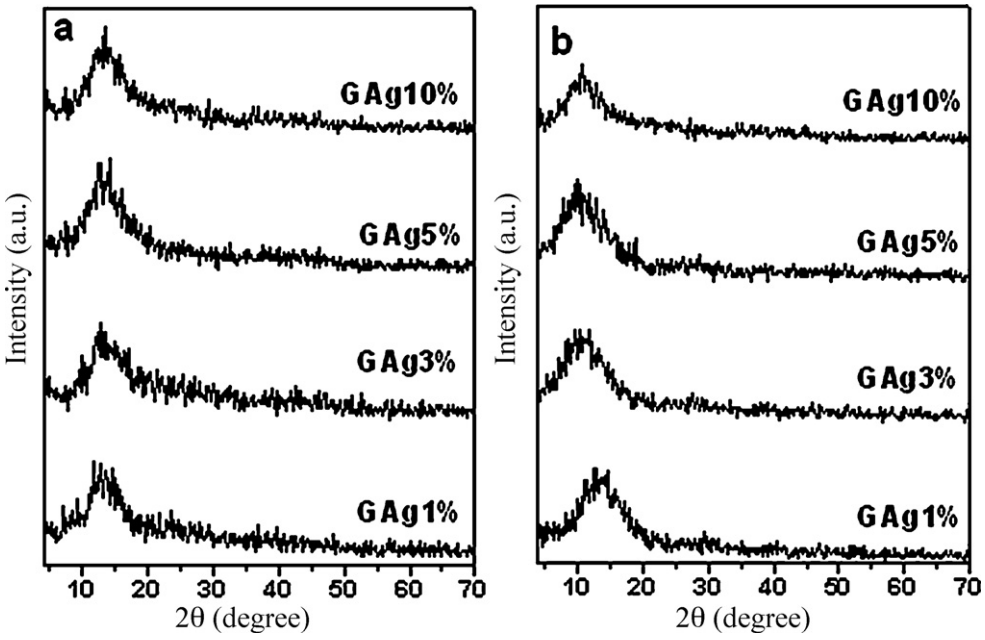

Fig. 5. The X-ray diffraction patterns of the as-prepared dry gels and after being calcined at 700 °C for 3 h.

0.38, 0.35, and 0.28 mg/L h^{-1}, respectively. The calculated correlation coefficients, R^2, of the cumulative silver released from samples GAg1%, GAg3% GAg5%, and GAg10% against the square root of time were 0.9867, 0.9903, 0.9877, and 0.9832, respectively. Those high values of the correlation coefficient indicated that silver releasing data perfectly fitted the heterogeneous model and varied with the square root of time. Therefore, the extraction of silver ions from the glasses followed a diffusion-controlled mechanism and could be predicted by Eq. (2).

Fig. 9 illustrates the cumulative concentration of silica ions released from the glasses versus time (a), as well as versus square root of time (b). The highest cumulative silica released was observed for sample GAg1% at 72, 168, and 336 h. On the other hand, the lowest one was observed for sample GAg10% at the same time periods. Sample GAg10% significantly ($p < 0.05$), released less silica than all the other samples that contained less silver at 72, 168, and 336 h. Therefore, the

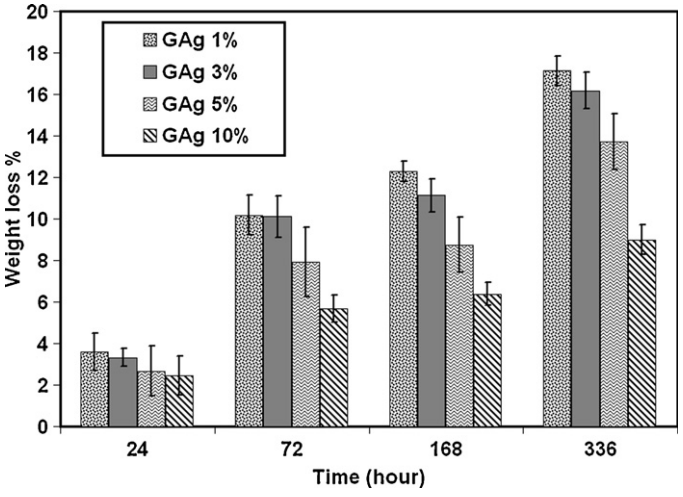

Fig. 6. The change of weight loss%, of sample GAg1%, GAg3%, GAg5%, and GAg10% with time of immersion in SBF, samples GAg1% and GAg3% had significantly ($p < 0.05$) greater weight losses than samples GAg5% and GAg10% at 72, 168, and 336 h.

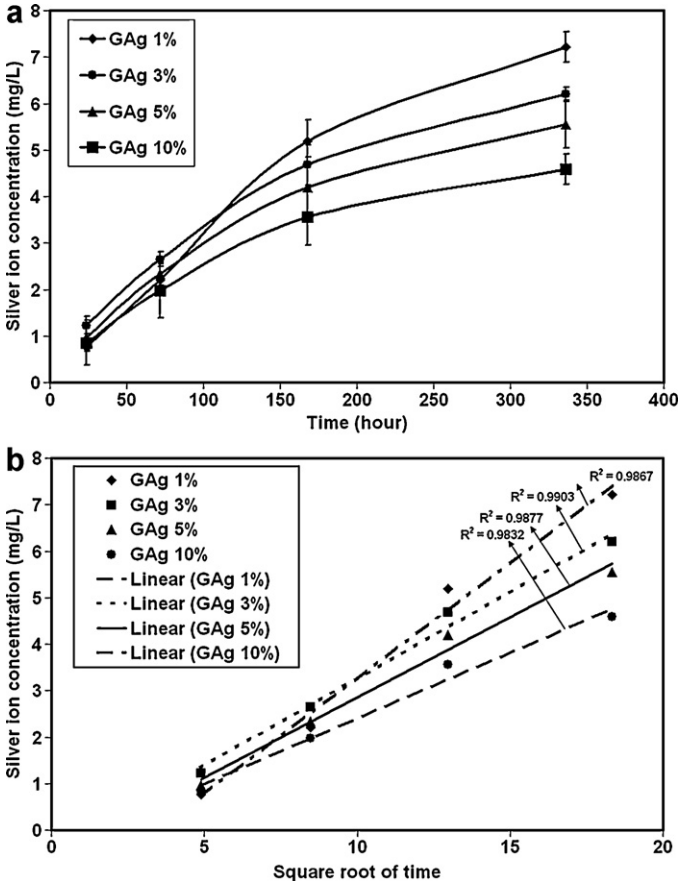

Fig. 7. The change of cumulative concentration of silver ion, released from all glass samples into SBF, with time (a) and with the square root of time (b).

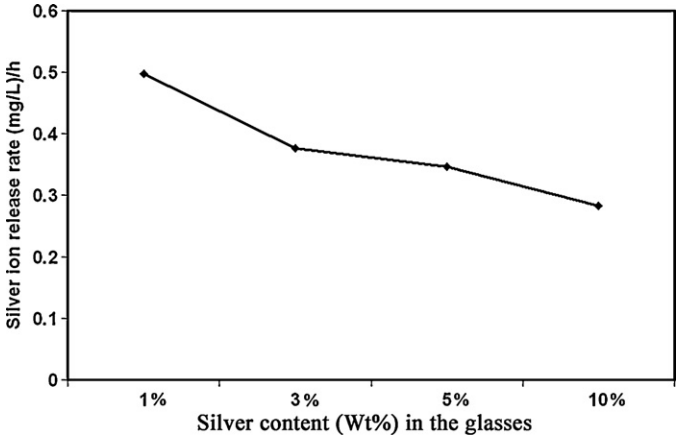

Fig. 8. The rate of silver release against silver content in the glasses.

addition of silver to glasses has affected their dissolution. The release rates of silica ions from the surfaces of glasses were 10.15, 9.41, 9.33, and 8.34 mg/L h^{-1} for GAg1%, GAg3%, GAg5% and GAg10%, respectively, indicating that the release rate was greatly affected by increasing their silver content. Sample GAg10% showed significantly ($p < 0.05$), lower silica ions release rate than sample GAg1%. The calculated correlation coefficients, R^2, of the cumulative silica released from samples GAg1%, GAg3%, GAg5% and GAg10% versus the square root of time were 0.9867, 0.9903, 0.9877, and 0.9832, respectively. Those values were very high and almost close to unity, indicating that the silica ions releasing data perfectly fitted the heterogeneous model and were varied with square root of time. Also the extraction of silica followed a diffusion-controlled mechanism.

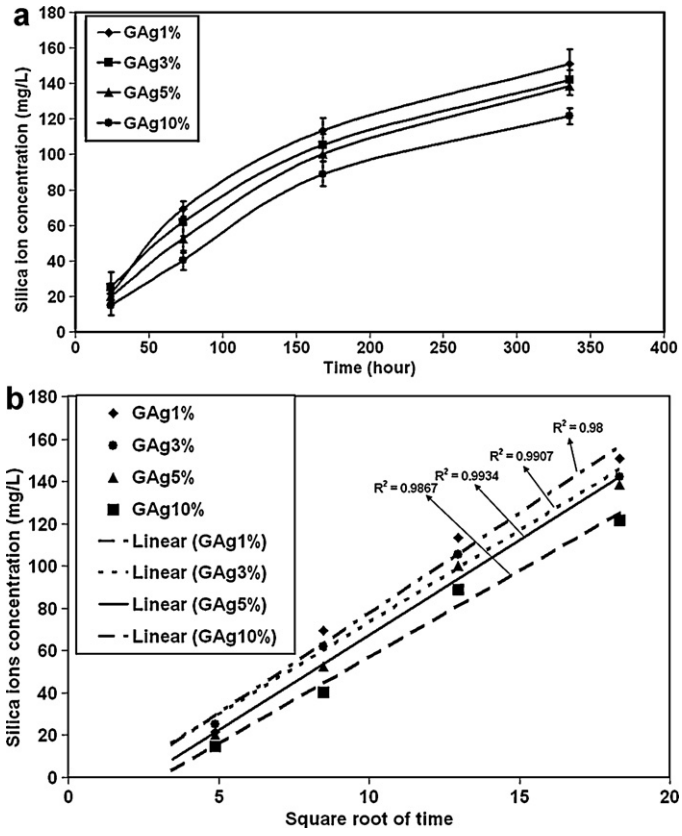

Fig. 9. Cumulative concentration of silica ion released versus time (a) and versus the square root of time (b).

3.3. Microbiological analysis

The Microbiological assay revealed that samples GAg1%, GAg3%, GAg5%, and GAg10% had an antibacterial effect against *Staphylococcus aureus* and *E. coli* as shown in Fig. 10(a) and (b), respectively. The figures demonstrate the inhibition zones around the glass disks in the agar plate after 24 h. The diameters of inhibition zones formed around all glass disks were more than 2 cm. Statistical analysis showed that, for the same type of bacteria, the difference in the measured diameters of inhibition zones around all glass disks (GAg1%, GAg3%, GAg5%, and GAg10%) were not significant. This was probably due to fact that, statistically, the extraction of silver ion from GAg1%, GAg3%, GAg5%, and GAg10% was not significant at 24 h as shown by their silver releasing profiles (see Fig. 7).

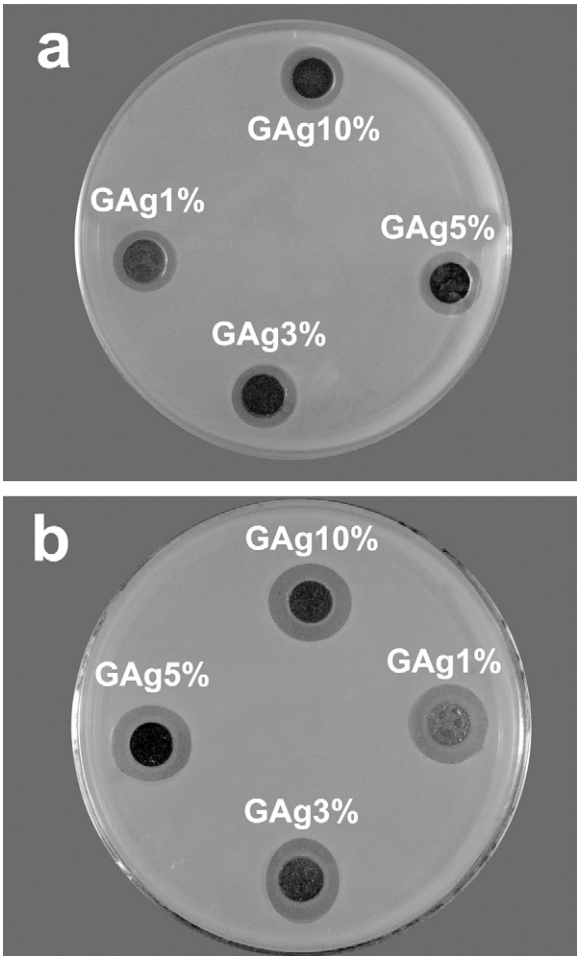

Fig. 10. The microbiological assay revealed that GAg1%, GAg3%, GAg5%, and GAg10% had an antibacterial effect against *Staphylococcus aureus* (a) and *E. coli* (b). The figure shows the inhibition zones around the glass disks in the agar plate after 24 h.

4. Discussion

In most sol–gel techniques, in order to synthesize silicate glass, sols were formed by the hydrolysis of tetraethoxysilane (TEOS) using water in presence of a catalyst. The hydrolysis reaction, replaced alkoxide groups with hydroxyl groups. Siloxane bonds (Si–O–Si) were then formed during the subsequent condensation. Further condensation leads to gelation which, after drying, forms a dry gel called xerogel. Alcohol and water were the byproducts of the condensation reaction and they evaporate during drying [38,39].

It is well known that the final size of the sol–gel derived powders greatly depends on the type of catalysts used. The catalyst influences the pH of the solution, and alters the relative rates of hydrolysis and condensation reactions [40]. Preparation of bioactive glasses by the traditional sol–gel process reported previously [7,11], using one-step acid catalysis, needed long gelation time, which allowed the aggregation and growth of colloidal particles in the solution and, hence, lead to a final product of particle sizes greater than 1 μm [41]. However, in our study, the traditional sol–gel process was modified by the addition of ammonia solution, therefore, a two-step acid–base catalysis was used. The addition of ammonia solution, as a second catalyst, to a sol that was initially catalyzed by nitric acid was found to increase the rate of condensation reactions and reduce the gelation time to few minutes. That is due to the fact that the condensation rate is proportional to $[OH^-]$ above the isoelectric point [42]. In our study, excess 2 M ammonia was used for gelation providing an environment of pH much higher than the isoelectric point of silica [40]. Hence gelation time was significantly decreased. Fast gelation of the sol and the application of a moderate ultrasonic dispersion combined with a mechanical agitation as well as the addition of ethanol as a dispersant in our study produced smaller grains of regular spherical shape if compared with the normal sol–gel conversion using only the acid hydrolysis route. Therefore, glass particles of less than 100 nm diameters were successfully prepared.

Textural analysis revealed that the glass nanoparicles were highly porous and had a relatively high surface areas. The sol–gel–derived nanopowders was characterized by mesopores ($2 <$ pore diameter < 50 nm). The porous nature of those materials originates from the manner by which the gel was formed. The alkoxide precursors react readily with water, and the hydrolyzed species link together in a condensation reaction. The liquid solvents that participated in the process were retained in the capillaries of the structure. The porosity of the glass was attributed to water and ethanol evaporation as well as to nitrate decomposition during the stabilization process that was carried out to convert the dry gel into glass. Those textural properties were shown by others to promote and accelerate the *in vitro* hydroxyapatite layer formation on the sol–gel derived bioactive glasses as compared with the melt-derived ones [7,13].

The degradation study carried out in this work showed that not only the weight losses% of the glasses were decreased, but also that the dissolution rates of silver and silica ions were decreased as the silver content was increased in their composition that could be due to the fact that the glass structure was very complex. The backbone of the silicate glass structure was the SiO_4 tetrahedral network. Those SiO_4 tetrahedral units were connected only at the oxygen ions at the corner to form a continuous 3D network. Alkali and alkaline earth oxides (Na^+, Ca^{+2}) serve to modify that network structure, and they reduce the degree of connectivity in the network by disruption of the continuity of the glassy network and replacing bridging oxygen groups which formed the link between two SiO_4 tetrahedral with non-bridging oxygen groups, i.e. the introduction of network modifiers to glass structure disrupts the network and promotes the formation of non-bridging oxygen groups. Those groups are very essential to facilitate the exchange of alkali or alkali-earth cations with H^+ or H_3O from the surrounding solution and increase the rate of glass dissolution [1]. An increase of glass alkali and alkaline earth content creates a large number of non-bridging oxygen groups in the glass structure, leading to a higher glass dissolution rate. In this study, calcium was replaced by silver in the glass structure, although both of them are glass modifiers, however calcium ions are divalent, and, therefore, one calcium ion was needed to produce two non-bridging oxygen groups in the silica network. On the other hand, silver ions are monovalent and two silver ions were needed to produce the same number of non-bridging oxygen groups that was produced by the introduction of one calcium ion. This means that replacing calcium with silver in the glass structure could reduce the number of non-bridging oxygen groups and decrease glass dissolution. Moreover, silver ion had greater electronegativity (1.93 Pauling unit) than calcium ion (1 Pauling unit). Electronegativity is a parameter originally introduced by Pauling which describes, on a relative basis, the tendency of an atom in a molecule to attract bonding electrons [43]. Hence, it is expected that the Ag–O bonds would be more covalent than that of Ca–O. Therefore, replacing calcium with silver in the glass structure would decrease the dissolution of the glass. To further confirm that silver addition has decreased glass dissolution, silica ions release rates were measured as an indication for glasses dissolution. Results revealed that as the silver content was increased in the glasses, the release rates of silica from their surfaces were decreased. Moreover, silver dissolution from the glasses was found to fit the heterogeneous model and, accordingly, its releasing rate could be exactly predicted, indicating the possibility to engineer glasses with specific and controlled silver dissolution rate that fits the patient needs simply by manipulating the silver content in it composition. Results of this study showed that GAg1%, GAg3% GAg5% and GAg10% had an anti-bacterial effect against different types of bacteria. This could demonstrate their ability to treat infection. The anti-bacterial effect of those glasses could be attributed to the silver ions released during their dissolutions. Bellantone et al. [44] investigated the effect of Ag_2O doped bioactive glasses on *S. aureus*, *E. coli*, and *P. aeruginosa*. The antibacterial action of the silver-doped bioactive glass was attributed to the leaching out of Ag^+ ions from the glass matrix. Feng et al. [45] studied the antibacterial effect of silver ions on *E. coli* and *S. aureus* and suggested that the antibacterial

mechanism was due to DNA not being able to replicate, and proteins were becoming inactivate after their contact with Ag^+. Kim et al. [46] suggested that Ag^+ ions interfered with the metabolism of the organism, thus inhibiting its growth. *In vitro and in vivo bioactivity* evaluation of the glass samples were currently underway to analyze their ability to induce an apatite layer on their surfaces and to regenerate bone tissue in animals.

5. Conclusion

Silver doped bioactive glass nanoparticles of different silver contents (1, 3, 5, 10 wt%) were successfully prepared using quick alkali mediated sol–gel method. Textural analysis revealed that all glass samples were highly porous and had relatively high surface area. The degradation study carried out in this work showed that not only the weight losses% for the glasses were decreased, but also that the dissolution rates of silver ions were decreased as the silver content increased in their composition. Dissolution study showed that the extraction of silver ions from all the glasses was a diffusion-controlled mechanism that fits the heterogeneous model and accordingly its releasing rate could be exactly predicted, indicating the possibility to engineer glasses with specific and controlled silver dissolution rates that fit the patient needs simply by manipulating the silver content in its composition. The microbiological assay revealed that all glass samples had an antibacterial effect against different type of bacteria, which could demonstrate their ability to treat bone infection.

References

[1] L.L. Hench, Bioceramics: from concept to clinic, J. Am. Ceram. Soc. 74 (1991) 1487.

[2] A. EL-Ghannam, P. Ducheyne, I.M. Shapiro, Bioactive material template for in vitro synthesis of bone, J. Biomed. Mater. Res. 29 (1995) 359.

[3] A. El-Ghannam, T. Abushusha, G. El-Bargeesy, A. Shama, D. El-Negmy, Surface modified bioactive glass enhances bone regeneration and graft material resorption in cortical and human maxillary cystic bone defects, Int. J. Oral Maxillofac. Implants 19 (2004) 2.

[4] C.A. Shapoff, D.C. Alexander, A.E. Clark, Clinical use of a bioactive glass particulate in the treatment of human osseous defects, Compendium 18 (1997) 352.

[5] L.L. Hench, Bioactive glasses and glass-ceramics, Mater. Sci. Forum 293 (1999) 37.

[6] J.P. Zhong, D.C. Greenspan, Processing and properties of sol–gel bioactive glasses, J. Biomed. Mater. Res. Appl. Biomater. 53 (2000) 694.

[7] P. Saravanapavan, L.L. Hench, Low temperature synthesis, structure and bioactivity of gel derived glasses in the binary $CaO–SiO_2$ system, J. Biomed. Mater. Res. 54 (2001) 608.

[8] H. Aguiar, J. Serra, P. Gonzālez, B. Le?ón, Structural study of sol–gel silicate glasses by IR and Raman spectroscopies, J. Non-Cryst. Solids 355 (2009) 475.

[9] R. Li, A.E. Clark, L.L. Hench, Chemical processing of advanced materials, John Wiley and Sons, New York, 1992.

[10] M.M. Pereira, A.E. Clark, L.L. Hench, Calcium phosphate formation on sol–gel-derived bioactive glasses in vitro, J. Biomed. Mater. Res. 28 (1994) 693.

[11] A. Saboori, M. Rabiee, F. Moztarzadeh, M. Sheikhi, M. Tahriri, M. Karimi, Synthesis, characterization and in vitro bioactivity of sol–gel-derived $SiO_2–CaO–P_2O_5–MgO$ bioglass, Mater. Sci. Eng. C 29 (2009) 335.

[12] A. Balamurugan, G. Balossier, S. Kannan, J. Michel, A.H.S. Rebelo, J.M.F. Ferreira, Development and in vitro characterization of sol–gel derived $CaO–P_2O_5–SiO_2–ZnO$ bioglass, Acta Biomater. 3 (2007) 255.

[13] D.C. Greenspan, J.P. Zhong, D.L. Wheeler, Bioactivity and biodegradability: melt vs sol–gel derived Bioglass® in vitro and in vivo, in: R.Z. LeGeros, J.P. LeGeros (Eds.), Bioceramics 11, 1998, 345 pp.

[14] S.A. Jones, P.G. Bowler, M. Walker, D. Parsons, Controlling wound bioburden with a novel silver-containing Hydrofiber dressing, Wound Repair Regen. 123 (2004) 288.

[15] S. Silver, L.T. Phung, Bacterial heavy metal resistance: new surprises, Annu. Rev. Microbiol. 50 (1996) 753.

[16] J.H. Crabtree, R.J. Burchette, R.A. Siddiqi, I.T. Huen, L.L. Handott, A. Fishman, The efficacy of silver-ion implanted catheters in reducing peritoneal dialysis-related infections, Perit. Dial. Int. 23 (2003) 368.

[17] G. Zhao, S.E. Stevens Jr., Multiple parameters for the comprehensive evaluation of the susceptibility of *Escherichia coli* to the silver ion, Biomaterials 11 (1998) 27.

[18] A. Yoshiki, M. Hiroshi, N. Iwao, S. Nobuko, A. Tomonori, Yutaka, S. Takafumi, Masaki, M. Masaaki, H. Takao, Calcium phosphate coating containing silver shows high antibacterial activity and low cytotoxicity and inhibits bacterial adhesion, Mater. Sci. Eng. C 30 (2010) 175–180.

[19] M. Catauro, M.G. Raucci, F.D. De Gaetano, A. Marotta, Antibacterial and bioactive silver-containing $Na_2O–CaO–2SiO_2$ glass prepared by sol–gel method, J. Mater. Sci. Mater. Med. 15 (2004) 831.

[20] A. Balamurugan, G. Balossier, D. Laurent-Maquin, S. Pina, A.H.S. Rebelo, J. Faure, J.M.F. Ferreira, An *in vitro* biological and anti-bacterial study on a sol–gel derived silver-incorporated bioglass system, Dent. Mater. 2 (4) (2008) 1343.

[21] P. Saravanapavan, J.E. Gough, J.R. Jones, L.L. Hench, Antimicrobial macroporous gel glasses: dissolution and cytotoxicity, Key Eng. Mater. 254–256 (2004) 1087.

[22] G. Balasunda, M. Sato, T.J. Webster, Using hydroxyapatite nanoparticles and decreased crystallinity to promote osteoblast adhesion similar to functionalizing with RGD, Biomaterials 27 (2006) 2798.

[23] L. Zhang, T.J. Webster, Nanotechnology and nanomaterials: promises for improved tissue regeneration, Nano Today 4 (2009) 66.

[24] T.J. Webster, C. Ergun, R.H. Doremus, R.W. Siegel, R. Bizios, Enhanced osteoclast-like cell functions on nanophase ceramics, Biomaterials 22 (2001) 1327.

[25] T.J. Webster, T.A. Smith, Increased osteoblast function on PLGA composites containing nanophase titania, J. Biomed. Mater. Res. A 74 (2005) 677.

[26] T.J. Webster, J.U. Ejiofor, Increased osteoblast adhesion on nanophase metals: Ti, Ti6Al4V, and CoCrMo, Biomaterials 25 (2004) 4731.

[27] C.Y. Chiang, S.H. Chiou, W.E. Yang, M.L. Hsu, M.C. Yung, M.L. Tsai, L.K. Chenf, H.H. Huang, Formation of TiO_2 nano-network on titanium surface increases the human cell growth, Dent. Mater. 2 (5) (2009) 1022.

[28] J. Li, Y. Dou, J. Yang, Y. Yin, H. Zhang, F. Yao, H. Wang, K. Yao, Surface characterization and biocompatibility of micro- and nano-hydroxyapatite/chitosan-gelatin network films, Mat. Sci. Eng. C 29 (2009) 1207.

[29] A.M. El-Kady, A.F. Ali, M.M. Farag, Development, characterization, and *in vitro* bioactivity studies of sol–gel bioactive glass/poly(L-lactide) nanocomposite scaffolds, Mat. Sci. Eng. C 30 (2010) 120.

[30] W. Xia, J.J. Chang, Preparation and characterization of nano-bioactive-glasses (NBG) by a quick alkali-mediated (sol–gel) method, Mater. Lett. 61 (2007) 325.

[31] T. Kokubo, H.M. Kim, M. Kawashita, H. Takadama, T. Miyazaki, M. Uchida, T. Nakamura, Nucleation and growth of apatite on amorphous phases in simulated body fluid, Glastech. Ber. Sci. Technol. 73C1 (2000) 247.

[32] M.G. Cerruti, D. Greenspan, K. Powers, An analytical model for the dissolution of different particle size samples of bioglass in TRIS-buffered solution, Biomaterials 2 (2005) 4903.

[33] I. Izquierdo-Barba, A.J. Salinas, M. Vallet-Regí, *In vitro* calcium phosphate layer formation on sol–gel glasses of the $CaO–SiO_2$ system, J. Biomed. Mater. Res. 47 (1999) 243.

[34] A. Oki, B. Parveen, S. Hossain, S. Adeniji, H. Donahue, Preparation and in vitro bioactivity of zinc containing sol–gel-derived bioglass materials, J. Biomed. Mater. Res. 69 (2004) 216.

[35] M. Vallet-Reg*ı*, A.M. Romero, C.V. Ragel, R.Z. LeGeros, XRD, SEM-EDS, and FTIR studies of *in vitro* growth of an apatite-like layer on sol–gel glasses, J. Biomed. Mater. Res. 44 (1999) 416.
[36] D. Arcos, D.C. Greenspan, M. Vallet-Reg, Influence of the stabilization temperature on textural and structural features and ion release in SiO_2–CaO–P_2O_5 sol–gel glasses, Chem. Mater. 14 (2002) 1515.
[37] N.J. Coleman, L.L. Hench, A gel-derived mesoporous silica reference material for surface analysis by gas sorption. 1. Textural features, Ceram. Int. 26 (2000) 171.
[38] J. Zhong, D.C. Greenspan, Processing and properties of sol–gel bioactive glasses, J. Biomed. Mater. Res. (Appl. Biomater.) 53 (2000) 694–701.
[39] L.L. Hench, J.K. West, The sol–gel process, Chem. Rev. 90 (1990) 33–72.
[40] C.J. Brinker, G.W. Scherer, The physics and chemistry of sol–gel processing, Academic Press Inc., San Diego, CA, USA, 1990.
[41] P. Sepulveda, J.R. Jones, L.L. Hench, Characterization of melt-derived 45S5 and sol–gel–derived 58S bioactive glasses, J. Biomed. Mater. Res. (Appl. Biomater.) 58 (2001) 734.
[42] C.J. Brinker, G.W. Scherer, Sol–Gel Science, Academic Press, Inc., 1990
[43] R.L. David, CRC Handbook of Chemistry and Physics, CRC Press, Boca Raton, 2005.
[44] M. Bellantone, H.D. Williams, L.L. Hench, Broad-spectrum bactericidal activity of Ag_2O-doped bioactive glass, Antimicrob. Agents Chemother. 46 (2002) 1940.
[45] Q.L. Feng, J. Wu, G.Q. Chen, F.Z. Cui, T.N. Kim, J.O. Kim, A mechanistic study of the antibacterial effect of silver ions on *Escherichia coli* and *Staphylococcus aureus*, J. Biomed. Mater. Res. 52 (2000) 662.
[46] T.N. Kim, Q.L. Feng, J.O. Kim, J. Wu, H. Wang, G.Q. Chen, F.Z. Cui, Antimicrobial effects of metal ions (Ag^+, Cu^{2+}, Zn^{2+}) in hydroxyapatite, J. Mater. Sci. Mater. Med. 9 (1998) 129.